

# A devil in the detail: parameter cross-talk from the solar cycle and estimation of solar p-mode frequencies

W. J. Chaplin<sup>1\*</sup>, S. J. Jiménez-Reyes<sup>1,2,†</sup>, A. Eff-Darwich<sup>3,2</sup>, Y. Elsworth<sup>1</sup>, R. New<sup>4</sup>

<sup>1</sup> School of Physics and Astronomy, University of Birmingham, Edgbaston, Birmingham, B15 2TT

<sup>2</sup> Instituto de astrofísica de Canarias, 38205, La Laguna, Tenerife, Spain

<sup>3</sup> Dept. Edafología Geología, Universidad de La Laguna, E-38205, Tenerife, Spain

<sup>4</sup> Faculty of Arts, Computing, Engineering and Sciences, Sheffield Hallam University, Sheffield S1 1WB

22 October 2018

## ABSTRACT

Frequencies, powers and damping rates of the solar p modes are all observed to vary over the 11-yr solar activity cycle. Here, we show that simultaneous variations of these parameters give rise to a subtle cross-talk effect, which we call the “devil in the detail”, that biases p-mode frequencies estimated from analysis of long power frequency spectra. We also show that the resonant peaks observed in the power frequency spectra show small distortions due to the effect. Most of our paper is devoted to a study of the effect for Sun-as-a-star observations of the low- $l$  p modes. We show that for these data the significance of the effect is marginal. We also touch briefly on the likely  $l$  dependence of the effect, and discuss the implications of these results for solar structure inversions.

## Key words:

Sun: helioseismology – Sun: interior – Methods: data analysis

## 1 INTRODUCTION

Long timebase observations of the “Sun as a star” made, for example, by the ground-based BiSON network (Chaplin et al. 2007) and the GOLF (Gabriel et al. 1995) and VIRGO/SPM (Fröhlich et al. 1997) instruments on the *ESA/NASA SOHO* spacecraft, provide key data on the low-degree (low- $l$ ) p modes for probing the deep solar interior and core. This paper is concerned chiefly with aspects of analysis of these Sun-as-a-star data.

Accurate and precise p-mode parameter data are a vital prerequisite for making robust inference on the interior structure of the Sun, and improved precision, and usually also improved accuracy, accrue from use of long helioseismic datasets (e.g., see discussion in Chaplin & Basu 2007). However, long helioseismic datasets must by necessity span a sizable fraction, or more, of an 11-yr solar activity cycle. Mode frequencies, damping rates, powers and peak asymmetries (Jiménez-Reyes et al 2007) all vary systematically with the solar cycle, and these variations can give rise to complications for the analysis and interpretation, with implications for parameter accuracies, when long datasets are analyzed in one piece.

There is the concern that changes in frequency over a long dataset may distort the underlying shapes of the mode peaks to such an extent that the shapes no longer match the Lorentzian-like functions that are used to model them. This ‘distortion’ effect turns out

not to be a significant cause for concern, at least where the Sun is concerned (Chaplin et al., 2008), although it may be an issue for stars that have shorter, and more pronounced, activity cycles than the Sun. There is, however, another potential problem for the solar observations, a ‘cross-talk’ effect that has its origins in the simultaneous variations of the mode frequencies, powers and linewidths over the solar cycle. This cross-talk effect can bias the estimated frequencies of the modes. The effect, which we call the “devil-in-the-detail”, is the subject of this paper.

To introduce the effect, let us begin with a fictitious scenario, in which the p-mode frequencies are the only mode parameters that are observed to vary over the solar cycle. A mode peak observed in the power frequency spectrum of a long dataset will then have a centroid frequency that corresponds to the unweighted average of its time-varying frequency, over the period of observation. This simple rule of thumb holds because the frequency shifts of the low- $l$  solar p modes are small, both in fractional terms and compared to the peak linewidths. In sum: the unweighted time-averaged frequency may be directly recovered.

Now consider what happens if the power of the mode is also observed to vary in time. This will mean that timeseries data at different epochs will have varying contributions to the final peak profile observed in the power frequency spectrum. Data samples from times when the mode is more prominent (i.e., at high power) will carry proportionately larger weights in determining the final peak profile than samples from times when the mode is less prominent (i.e., at low power). Because the frequency also varies in time, one

\* E-mail: w.j.chaplin@bham.ac.uk

† E-mail: sjimenez@iac.es

would expect the mode peak to be pulled, or biased, to a lower or higher frequency than the unweighted average frequency, with the size and sign of the effect dependent on the comparative time variations of the frequency and power. This is our devil in the detail.

Why might the devil in the detail matter? First, it raises uncertainty over what it is we are actually measuring when we determine mode frequencies from long datasets. If we have two sets of data that are not contemporaneous, it creates uncertainty if we wish to correct their frequencies to a common level of activity. Correction procedures, which attempt to ‘remove’ the solar-cycle effects from the fitted frequencies, can be quite sophisticated (e.g., the BiSON correction procedure; see Basu et al. 2007); but they assume that the observed mode frequencies correspond to unweighted time averages of the frequencies. The devil-in-the-detail effect means this is not true in practice. Furthermore, because the frequency bias that is introduced depends on the relative sizes of the parameter variations – the larger the fractional power variation, for a given frequency variation, the more pronounced the effect – we might also expect there to be some dependence of the bias on the angular degree,  $l$ . Both issues above have potential implications for structure inversions made with the estimated p-mode frequencies.

The layout of the rest of the paper is as follows. In Section 2, we spell out why cross-talk from simultaneous variations of the mode parameters introduces the devil-in-the-detail bias in estimation of frequencies from Sun-as-a-star data. We then describe how artificial data were used to illustrate, and quantify, the problem. We give some important background on the Sun-as-a-star observations in Section 3.1, and details on the artificial Sun-as-a-star data in Section 3.2. We then discuss results from analysis of long (9.5-yr) artificial datasets in Section 4, where we attempt to quantify the likely size of the devil-in-the-detail effect for real observations. Finally, we pull together the main points of the paper in Section 5, where we discuss the implications for analysis of real data. We also touch on the issue of the  $l$  dependence of the effect, and the possible impact on results of structure inversions.

## 2 THE DEVIL IN THE DETAIL: PARAMETER CROSS-TALK AND THE SOLAR CYCLE

To illustrate the devil-in-the-detail effect, and its impact on the observed mode profiles in the power frequency spectrum, we begin by making use of Monte Carlo simulations of single artificial p modes. We consider simulations of full Sun-as-a-star datasets later in Section 3.

The Laplace transform solution of the equation of a forced, damped harmonic oscillator was used to generate mode components at a 40-s cadence in the time domain, in the manner described by Chaplin et al. (1997). Components were re-excited independently at each sample with small ‘kicks’ drawn from a Gaussian distribution. The simulations gave modes having Lorentzian limit shapes in the power frequency spectrum. Simulation of the data in the time domain allowed us to introduce small, time-dependent perturbations of the oscillation parameters to simulate the effects of the solar-cycle parameter shifts. We consider in this section sets of simulation results where parameter shifts were introduced as simple linear functions in time,  $t$ . The frequencies in each timeseries of length  $T$  were perturbed linearly according to:

$$\nu(t) = \nu(0) + \Delta\nu t/T, \quad (1)$$

where  $\nu(0)$  was the initial frequency of the mode, and the constant

$\Delta\nu$  fixed the full increase in  $\nu(t)$  from the beginning to the end of the timeseries.

The quantity of interest for measuring the prominence of a mode in the power frequency spectrum is the maximum power spectral density, or height  $H$ , of the resonant peak. There are two independent ways in which the height may be varied in time. First, the energy given per unit time to the oscillator may be varied, for example by systematic variation of the standard deviation describing the excitation ‘kicks’. This first scenario leads to changes in height, but the damping rate, and therefore the peak width  $\Gamma$ , remains fixed. In the second scenario the damping rate is varied, while the energy given per unit time to the oscillator remains fixed. This second approach leads to variation over time of the width *and* the height of the resonant peak. The fractional variation in the height is twice that in the width, and the fractional changes have opposite sign. More details on the oscillator variations may be found in Appendix A.

On the Sun, an increase in the surface activity brings with it an increase in the frequency and damping rate, and a decrease in the height (and total power) of a typical low- $l$  mode. Indeed, the observed sizes and signs of the solar-cycle variations of the low- $l$  mode parameters appear to be consistent with the second scenario above (Chaplin et al. 2000), where just the damping is varied, and the underlying excitation is unchanged over time. Here, we still tested both scenarios to demonstrate that the size of the devil-in-the-detail bias introduced in the observed mode frequencies depends on the scenario that is used.

In both scenarios variation of the excitation or damping parameter was contrived in such a way as to give an implied linear variation of the height over time, i.e.,

$$H(t) = H(0) - \Delta H t/T. \quad (2)$$

In the above,  $\Delta H$  describes the full decrease in  $H(t)$ , from  $t = 0$  to  $t = T$ . We averaged 10,000 independent realizations for computations made at each chosen combination of  $\Delta\nu$  and  $\Delta H$ , to recover estimates of the underlying profiles. Some averaged profiles, which have also been subjected to a small amount of boxcar smoothing (boxcar width  $\sim 0.3 \mu\text{Hz}$ ), are plotted in Fig. 1. All artificial datasets used to make this plot simulated a mode having an unperturbed frequency of  $\nu(0) = 3000 \mu\text{Hz}$ , an unperturbed linewidth of  $\Gamma(0) = 1 \mu\text{Hz}$ , and a frequency shift  $\Delta\nu = 0.40 \mu\text{Hz}$ .

The curves in the left-hand panel show results for simulations made under the first scenario: here, the amplitude of the excitation was varied over time. The profile drawn as the solid line in the figure shows the average peak for modes which had no height variation, i.e.,  $\Delta H = 0$ . The other linestyles show results for fractional height changes,  $\Delta H/H(0)$ , of:  $-0.25$  (dotted),  $-0.50$  (dashed) and  $-0.80$  (dot-dashed) respectively. Note that the dotted curve has a  $\Delta H/H(0)$  very similar to that seen for the most prominent low- $l$  p modes between solar minimum and maximum. The curves in the right-hand panel show results for simulations made under the second scenario: here, the damping rate was varied over time. The various linestyles show results for the same  $\Delta H/H(0)$  as the left-hand panel.

The curves in Fig. 1 show clear, and predictable, trends. In the absence of any height variation (solid curves) modes are shifted in frequency by  $\Delta\nu/2$ , i.e., the shift is determined by the (unweighted) average size of the perturbation. However, when variation in  $H$  is introduced (other linestyles) the mode peaks are shifted in frequency by amounts less than  $\Delta\nu/2$ . This is the devil-in-the-detail effect. In order to explain the effect, we must remember that as  $t$  increased in our artificial timeseries, the  $H$  decreased while at the same time the frequencies increased. Data samples from times

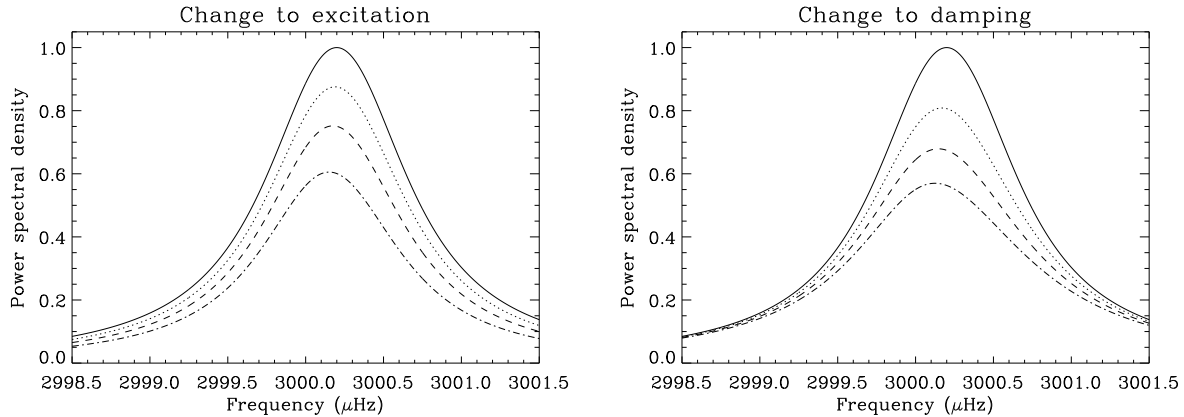


**Figure 1.** Results on simulations of single, artificial  $p$  modes in timeseries where the frequency shift, from start to end, was  $0.40 \mu\text{Hz}$ . Each curve shows the average profile given by co-adding the power frequency spectrum of 10,000 independent realizations (the co-added spectra were also smoothed with a boxcar of width  $\sim 0.3 \mu\text{Hz}$ ). Results in the left-hand panel are for the first simulation scenario, where the amplitude of the excitation was varied over time; results in the right-hand panel are for the second scenario, where the damping rate was varied over time. The profile drawn as the solid line in each panel shows the average peak for modes which had no height variation over time, i.e.,  $\Delta H = 0$ . The other linestyles show results for fractional height changes,  $\Delta H/H(0)$ , of:  $-0.25$  (dotted),  $-0.50$  (dashed) and  $-0.80$  (dot-dashed).

when frequencies were lower therefore carried a proportionately larger weight in determining the final peak profiles. We may therefore also say that the effect arises from cross-talk between the time-varying mode parameters.

The final profiles are in fact well described by the integral over time of instantaneous Lorentzian profiles sampled at times  $t$ , having the appropriate frequency, height and damping rate for that time, i.e.,

$$\langle P(\nu) \rangle = \frac{1}{T} \int_{t=0}^T \frac{H(t)}{1 + \xi^2(t)} dt, \quad (3)$$

where

$$\xi(t) = 2[\nu - \nu(t)]/\Gamma(t). \quad (4)$$

Under the first scenario, where the amplitude of the excitation is varied but the damping remains fixed (left-hand panel of Fig. 1), the frequency of the final profile is well described by a simple, linear weighted summation of the instantaneous frequencies,  $\nu(t)$ , where the weights are proportional to  $H(t)$ . That the simple weighting should take this form is clear from Equation 3. However, under the second scenario, where the damping is varied but the excitation amplitude remains fixed (right-hand panel of Fig. 1), this simple relation no longer holds because the final profile is also affected by the change in the damping over time (again, see Equation 3).

The devil-in-the-detail effect also gives rise to small changes in the shapes of the peak profiles. First, due to changes in frequency the widths of the peaks are increased compared to the basic input widths (first scenario) or the (unweighted) average widths (second scenario). Second, the peaks are observed to be slightly asymmetric: there is slightly more power present on the high-frequency side of the peaks compared to the low-frequency side. The asymmetry increases in size as  $\Delta H/H(0)$  is increased. And for a given  $\Delta H/H(0)$ , the asymmetry for the second scenario is larger than the asymmetry for the first scenario.

How large is this peak asymmetry? Let us define the asymmetry of a peak to be:

$$\langle B \rangle = \frac{\langle H \rangle_{+(\Gamma/2)} - \langle H \rangle_{-(\Gamma/2)}}{2 \langle H \rangle}. \quad (5)$$

Here  $\langle H \rangle$  is the height of the peak profile; and  $\langle H \rangle_{+(\Gamma/2)}$  and  $\langle H \rangle_{-(\Gamma/2)}$  are the heights of the peak at frequencies plus and minus half the linewidth. (Equation 5 is consistent with the asymmetry parameter in the well-used Nigam & Kosovichev (1998) asymmetric fitting formula, provided the second-order asymmetry terms in the fitting formula are ignored; see also Toutain, Elsworth & Chaplin 2006.) The asymmetry of the final peaks shown in Fig. 1 rises to 0.2 per cent (first scenario; left-hand panel) and 1.4 per cent (second, right-hand panel), respectively, when  $\Delta H/H(0) = -0.8$ . We discuss the expected contributions to the asymmetries of real  $p$ -mode peaks later in Section 4.3.

To summarize, significant variation in the height of a mode over time is expected to give rise to a cross-talk effect with the frequency parameter. In the absence of such variation, the location in frequency of the centroid of the mode peak (in the power frequency spectrum) would in principle give an accurate measure of the unweighted average mode frequency over the period of observation. However, when significant variation of the height is present, the peak of the mode will be pulled to a slightly lower frequency, and it cannot be assumed that the estimated frequency is the unweighted average frequency. Some distortion of the underlying peak shape is also expected.

Next, we go on to ask: How large, and how significant, are the effects for the low- $l$  solar  $p$  modes?

### 3 ARTIFICIAL SUN-AS-A-STAR DATA

In order to quantify the likely impact of the devil-in-the-detail effect described above on real observations, we generated, and then analyzed, 40 artificial datasets each of which was designed to mimic just under 9.5 yr of full BiSON or GOLF-like Sun-as-a-star Doppler velocity observations. In order to understand some of the results one first has to understand the basic characteristics of the Sun-as-a-star data. We discuss these characteristics next (Section 3.1) before going on to give more details on the full artificial datasets in Section 3.2. Those who are very familiar with the Sun-as-a-star data should be safe skipping Section 3.1.

### 3.1 Sun-as-a-star observations

Sun-as-a-star observations take an average, over the visible disc, of either the Doppler velocity or intensity perturbations associated with the modes. The technique is inherently very stable and shows excellent sensitivity to the low- $l$ , core-penetrating modes. When the observations are made from a location in, or close to, the ecliptic plane the rotation axis of the Sun is always nearly perpendicular to the line-of-sight direction, and only some of the  $2l + 1$  components of the non-radial modes are clearly visible: those having even  $l + m$ , where  $m$  is the azimuthal order. This is the perspective from which the Sun-as-a-star BiSON (ground-based network), and GOLF and VIRGO/SPM (on the SOHO spacecraft at L1), view the Sun.

A set of Sun-as-a-star observations gives a single time series whose power frequency spectrum contains many closely spaced mode peaks. Parameter estimation must contend with the fact that within the non-radial mode multiplets the various  $m$  lie in very close frequency proximity to one another. Suitable models, which seek to describe the characteristics of the  $m$  present, must therefore be fitted to the components simultaneously. Furthermore, overlap between modes adjacent in frequency is a cause for concern over much of the low- $l$  spectrum (in particular at high frequencies, where the mode peaks are wider due to heavier damping).

Let us consider the impact of the solar activity cycle. The mode parameters are observed to vary over time, in response to variations of the near-surface activity. Estimates of the parameters depend not only on when the observations were made, but also on the frequencies, and the spatial properties [i.e., the  $(l, |m|)$ ], of the modes. The frequencies matter because the mode inertias are frequency dependent, and the inertias affect the sensitivity of the modes to the near-surface perturbations. The spatial properties matter because the distribution of the near-surface activity is spatially non-homogeneous. The response of the modes to the changing activity is therefore in part determined by the combination  $(l, |m|)$ . This spatial dependence, in combination with the visibility characteristics of the Sun-as-a-star data, creates a complication that has already been well documented in the literature (e.g., Chaplin et al. 2004). We raise this complication here because it plays a part in understanding results on the devil-in-the-detail effect, presented later in Section 4.1.

The complication arises for modes with  $l \geq 1$ , because then some of the mode components are no longer visible in the Sun-as-a-star data (see above). Since these components are in effect missing from the observations, and those components that are present have solar-cycle frequency shifts that are  $(l, |m|)$ -dependent, it is not possible to estimate accurately the frequency centroids of the non-radial modes. It is the centroids that carry information on the spherically symmetric component of the internal structure, and which are therefore required as input for the hydrostatic structure inversions. In the complete absence of the near-surface activity, the missing components would be an irrelevance. All mode components would then be arranged symmetrically in frequency, meaning centroids could be estimated accurately from the subset of components visible to the Sun-as-a-star data. A near-symmetric arrangement is found at the epochs of the modern cycle minima. However, when the observations span a period showing medium to high levels of activity – as a long dataset by necessity must – the frequencies given by fitting the Sun-as-a-star data differ from the true centroids by an amount that is sensitive to  $l$ . This  $l$  sensitivity arises because modes of different  $l$  are comprised of visible components having different combinations of  $l$  and  $|m|$ ; and these different combina-

tions show different solar-cycle frequency shifts (in amplitude and phase).

The ‘complication’ outlined above is important for what follows, in that we first had to quantify the  $l$  dependence of the frequencies introduced by it, in order to properly isolate the devil-in-the-detail effect. This was done using artificial datasets simulating full Sun-as-a-star observations. Next, we go on to describe how the datasets were made.

### 3.2 The full artificial datasets

Each of the full artificial datasets had a simulated length of 3456 days ( $\sim 9.5$  yr), and was constructed component by component in the time domain (in the manner described for single  $p$  modes in Section 2 above). Sets were made with a full cohort of simulated low- $l$  modes, covering the ranges  $0 \leq l \leq 5$  and  $1000 \leq \nu \leq 5500 \mu\text{Hz}$ . The artificial datasets were given the same underlying parameters as the datasets used for the first hare-and-hounds exercise of the solarFLAG<sup>1</sup> collaboration. All datasets had different realization noise. More details on how the datasets were made may be found in Chaplin et al. (2006).

Solar-cycle-like variations were introduced through systematic variation in simulated time of the oscillator parameters. A high-order polynomial fit to the disc-averaged solar 10.7-cm radio flux, observed over the 9.5-yr period beginning 1992 July 24, was used to describe the globally averaged activity of our artificial Sun. We used known sensitivities of the  $p$ -mode parameters to variations in the 10.7-cm flux to calibrate the simulated time variations of the oscillator parameters.

We introduced systematic changes in mode frequency, which had an appropriate underlying  $(l, |m|)$  and frequency dependence. This was accomplished through appropriately scaled variation (see, for example, Jiménez-Reyes et al 2004) of the frequency parameter of each component. Solar-cycle-like changes were also introduced in the component damping rates and powers. These changes were given a weak frequency dependence (as seen in real observations), but no dependence on  $(l, |m|)^2$ .

We constructed two sequences of artificial data. Each sequence was comprised of 20 independent artificial realizations of a 9.5-yr dataset. In the first sequence, which we call sequence FLAG#0, solar-cycle-like variations were introduced *only* in the mode frequencies. Datasets in the second sequence, which we call sequence FLAG#1, had variations in mode frequency *and* mode damping and mode power.

To illustrate visually the effect given to one of the mode peaks under these more realistic simulation scenarios, Fig. 2 shows profiles for the  $l = 0, n = 21$  mode ( $\nu(0) = 3033.7 \mu\text{Hz}$ ). The solid line shows the final peak for the FLAG#0 scenario; and the dotted line the final peak for the FLAG#1 scenario. The FLAG#1 peak has an asymmetry of 0.4 per cent (see also Fig. 5 and discussion at end of Section 4.3).

<sup>1</sup> solarFLAG URL: <http://bison.ph.bham.ac.uk/~wjc/Research/FLAG.html>

<sup>2</sup> Only recently (Salabert et al. 2007) has evidence for an  $(l, |m|)$ -dependence of the excitation and damping parameters been uncovered in the low- $l$  modes, and only then at marginally significant levels.

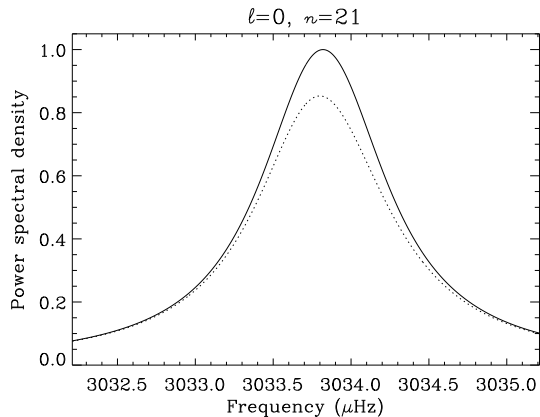


**Figure 2.** Final peaks for artificial  $l = 0$ ,  $n = 21$  mode, in artificial power spectra made from 9.5-yr of simulated Sun-as-a-star oscillations data. The solid line shows the final peak for the FLAG#0 simulation scenario; and the dotted line the final peak for the FLAG#1 scenario (see text).

## 4 ANALYSIS OF FULL 9.5-YR DATASETS

### 4.1 Overview and basic results

The 9.5-yr datasets were analysed in their entirety. This meant we first computed the power frequency spectrum of each full dataset. Multi-component models were then fitted to modes in each power frequency spectrum to extract estimates of the mode parameters. This was accomplished by maximizing a likelihood function commensurate with the  $\chi^2$ , 2-d.o.f. statistics of the power spectral density. We adopted the usual approach to fitting the Sun-as-a-star spectra (e.g., see Jiménez-Reyes et al 2007), and the low- $l$  modes were fitted in pairs ( $l = 0$  with 2, and  $l = 1$  with 3) in the range  $1400 \leq \nu \leq 3500 \mu\text{Hz}$ . This is the range over which it is possible to extract well-constrained estimates of the solar-cycle frequency shifts in the real observations. To reduce uncertainties, the fitted frequencies of each mode were averaged over the 20 datasets in each sequence, to give two final sets of mean fitted mode frequencies.

Fig. 3 summarizes the main results of this full-spectrum exercise. The frequency residuals plotted as symbols for different  $l$  (see annotation) are differences between the mean fitted mode frequencies and the unperturbed input mode frequencies (with FLAG#0 differences shown in left-hand panel, and FLAG#1 differences shown in the right-hand panel). By unperturbed frequencies, we mean the underlying input frequencies onto which the solar-cycle-like variations were added in the artificial data. The unperturbed frequencies may therefore be regarded as notional “zero-activity” frequencies. We have also plotted the errors on the  $l = 0$  mean fitted frequencies, to give a guide to the precision in the data (uncertainties on the mean frequencies at the other  $l$  have similar sizes). The first point to take from the figure is that the mean fitted frequencies exceed the unperturbed, zero-activity frequencies by amounts that depend on both frequency and degree,  $l$ . These differences are of course due to the solar-cycle frequency shifts that we introduced in the data.

The various lines in the both panels show the unweighted average frequency shifts that were actually introduced (see annotation). For each mode, this shift is just the difference between the unweighted average of the time-varying frequency over the 9.5-yr simulated observation, and the unperturbed input frequency. How were these average frequency shifts calculated? Calculation of the

average shifts is trivial for the  $l = 0$  and 1 modes, because only one combination of  $(l, |m|)$  components is observed in the Sun-as-a-star (and hence our artificial) data at these degrees. The shifts are given by the unweighted average frequency shifts of the (0,0) and (1,1) components, respectively, over period of simulated observation, and these are plotted as solid and dotted lines in both panels of Fig. 3.

At  $l = 2$  and 3 matters are non-trivial, because of the ‘complication’ we discussed at the end of Section 3.1 above. Here, modes seen in the Sun-as-a-star observations are comprised of components showing two different combinations of  $l$  and  $|m|$ , each of which has a different-sized shift over the solar cycle. How should the expected shifts be computed for these modes? Chaplin et al. (2004) showed that the fitted  $l = 2$  and 3 Sun-as-a-star frequencies may be modelled as linear combinations of the frequencies of the visible  $(l, |m|)$ . These combinations turn out to be dominated by the frequencies of the outer  $|m| = l$  components, because they are more prominent than the other visible components in the multiplets. More recently, Appourchaux & Chaplin (2007) have given frequency-dependent estimates of the coefficients that are needed to scale the combinations at each  $l$ . In effect, use of the coefficients allows one to calculate a notional Sun-as-a-star frequency for every mode at  $l = 2$  and  $l = 3$ , from an appropriate combination of the frequencies of the constituent  $m$ . This we have done here, to give unweighted Sun-as-a-star averages of the time-varying  $l = 2$  and 3 frequencies, from which the unweighted average frequency shifts plotted as dashed and dot-dashed lines in both panels of Fig. 3 were calculated. By applying this procedure, we take care of the  $l$  dependence of the frequencies introduced by the missing components, and therefore our ‘complication’.

What are the main conclusions to be drawn from the results plotted in Fig. 3? The data plotted in the left-hand panel show that the fits to the FLAG#0 data recover the unweighted average frequency shifts, and therefore the unweighted average frequencies, at the level of precision of the simulated observations. Recall that only the frequencies were varied over time in these datasets. There are, in contrast, significant discrepancies present in the FLAG#1 results. This is of course due to the devil-in-the-detail effect. The FLAG#1 datasets included within them variations over time of the heights and widths of the modes. These variations in effect gave a different weighting to different parts of the timeseries, resulting in a systematic underestimation of the unweighted average frequencies, just as was seen in the simpler, linear-shift simulations in Section 2.

To get a quantitative measure of the cumulative significance of the differences we did the following. We performed a linear regression of the FLAG#0 and FLAG#1 mean fitted frequency residuals (various symbols in Fig. 3) on the unweighted average frequency shifts (various linestyles). The data in Table 1 correspond to the best-fitting gradients for each  $l$ . A best-fitting gradient of unity is expected when the fitted frequencies match the average input frequencies. Gradients consistent with unity are returned from analysis of the FLAG#0 data<sup>3</sup>. However, for FLAG#1 all gradients lie

<sup>3</sup> Recall that at  $l = 2$  and 3 the unweighted average frequency shifts were computed from weighted linear combinations of the unweighted average shifts of the different  $|m|$  seen in these modes. The different  $|m|$  seen are:  $|m| = 2$  and 0 at  $l = 2$ ; and  $|m| = 3$  and 1 at  $l = 3$ . If the weaker, inner components are neglected, and only the average shifts of the outer components are used, the FLAG#0 best-fitting gradients are reduced at  $l = 2$  and 3 to 0.92 and 0.90, respectively. This emphasizes that allowance must be made for the influence of the weaker, inner components on the fits when the expected average shifts are estimated.

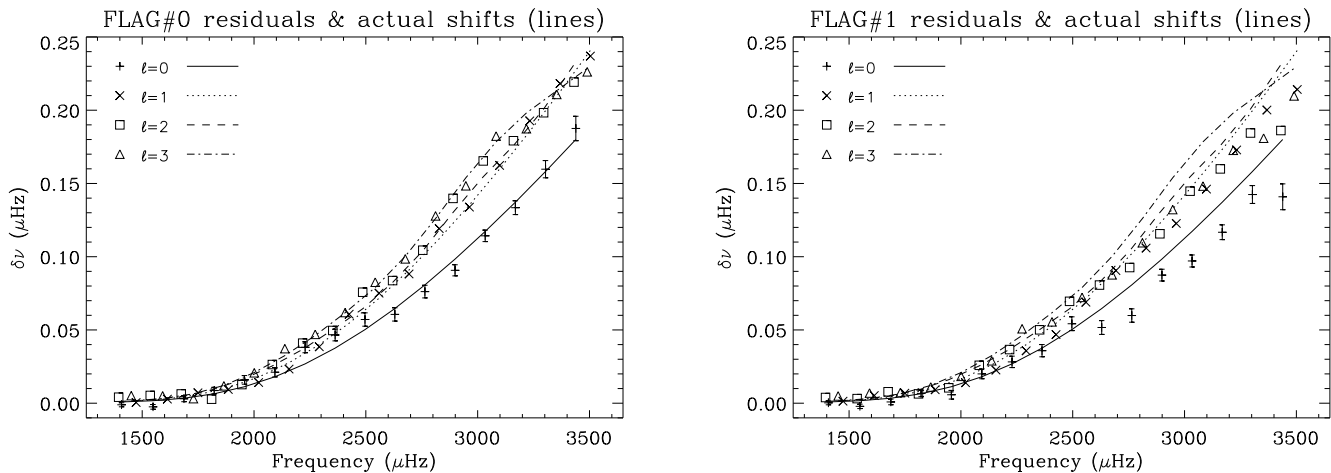


**Figure 3.** Main results of the full-spectrum exercises (Section 4) for the FLAG#0 (left-hand panel) and FLAG#1 (right-hand panel). Frequency residuals plotted as symbols for different  $l$  (see annotation) are differences between the full-spectrum mean fitted mode frequencies and the unperturbed (“zero activity”) input mode frequencies. The residuals are due to the solar-cycle frequency shifts introduced into the data. The various lines (see annotation) show the unweighted average frequency shifts that were introduced in the data (i.e., for a given mode, the difference between the unweighted average of the time-varying frequency over the 9.5-yr simulated observation, and the unperturbed input frequency).

**Table 1.** Results of performing a linear regression of the FLAG#0 and FLAG#1 fitted frequency residuals on the unweighted average frequency shifts present in the datasets. The results in the table correspond to the best-fitting gradients.

Degree, $l$	Best-fitting gradient	
	FLAG#0	FLAG#1
0....	$1.00 \pm 0.02$	$0.86 \pm 0.02$
1....	$1.02 \pm 0.01$	$0.92 \pm 0.02$
2....	$1.01 \pm 0.02$	$0.89 \pm 0.02$
3....	$0.98 \pm 0.02$	$0.84 \pm 0.02$

significantly below unity, by anywhere from 5 and  $8\sigma$ , because the average input frequencies are systematically underestimated.

#### 4.2 Size of the devil-in-the-detail effect

The frequency bias introduced by the devil-in-the-detail effect corresponds to the amounts by which the fitted frequencies underestimate the unweighted average frequencies. This bias may therefore be estimated directly by subtracting the mean fitted FLAG#1 frequencies from the mean fitted FLAG#0 frequencies. When we perform this subtraction, we obtain the bias estimates plotted as crosses with error bars in Fig. 4.

How significant is the bias? We have also plotted in each panel of this figure the sizes of the typical frequency uncertainties expected from a single 9.5-yr dataset (dashed lines). The plots show that the bias for individual modes is typically smaller in size than the frequency uncertainties. That said, the bias is systematic, and the cumulative effect is undoubtedly significant (e.g., see data in Table 1).

Finally, we are also in a position to predict the devil-in-the-detail frequency bias. This may be accomplished numerically, by using Equation 3 to construct the expected final profiles of each mode peak for the known FLAG#1 input parameters, and input parameter variations. Comparison of the frequency maxima of these

calculated profiles with the unweighted average frequencies then gives the expected bias. The resulting predictions are plotted as dotted lines in each panel of Fig. 4. Fair agreement is seen with the results given by fitting the artificial data (crosses with errors), although offsets are present, most notably in the higher frequency range. These offsets presumably reflect the impact of other subtle bias effects that the Sun-as-a-star fits are subject to.

#### 4.3 Effect on peak shape

We recall from Section 2 that the devil-in-the-detail effect should also give rise to peak asymmetry. Fig. 5 plots the peak asymmetry given to the  $l = 0$  modes in the 9.5-yr FLAG#1 simulations. We re-emphasize that this asymmetry comes from the interplay of the variations in frequency, power and damping over the simulated 9.5-yr period of observation.

Observations of the real low- $l$  modes show peak asymmetry that is close to zero at frequencies of  $\sim 3000 \mu\text{Hz}$ . The asymmetry increases in size to a few per cent at the extreme ends of the visible p-mode spectrum. The asymmetry is also negative in the Doppler velocity data, i.e., there is more power observed on the low-frequency side of the peaks. The data plotted in Fig. 5 provide a guide to that part of the observed asymmetry of the real solar p modes that might be expected to come from the devil-in-the-detail effect, assuming the real observations to be of similar length, and to cover similar levels of activity, as the artificial data here.

The devil-in-the-detail contribution is seen to be smallest at both ends of the plotted frequency range, where the real observed asymmetries happen to take their largest values. We would therefore not expect there to be a significant bias in the asymmetries in these parts of the spectrum. However, the observed asymmetries of the modes near the centre of the spectrum are much smaller in magnitude, and this is where the devil-in-the-detail asymmetry contribution has its largest values. We might therefore expect a more significant bias in this central part of the p-mode spectrum.

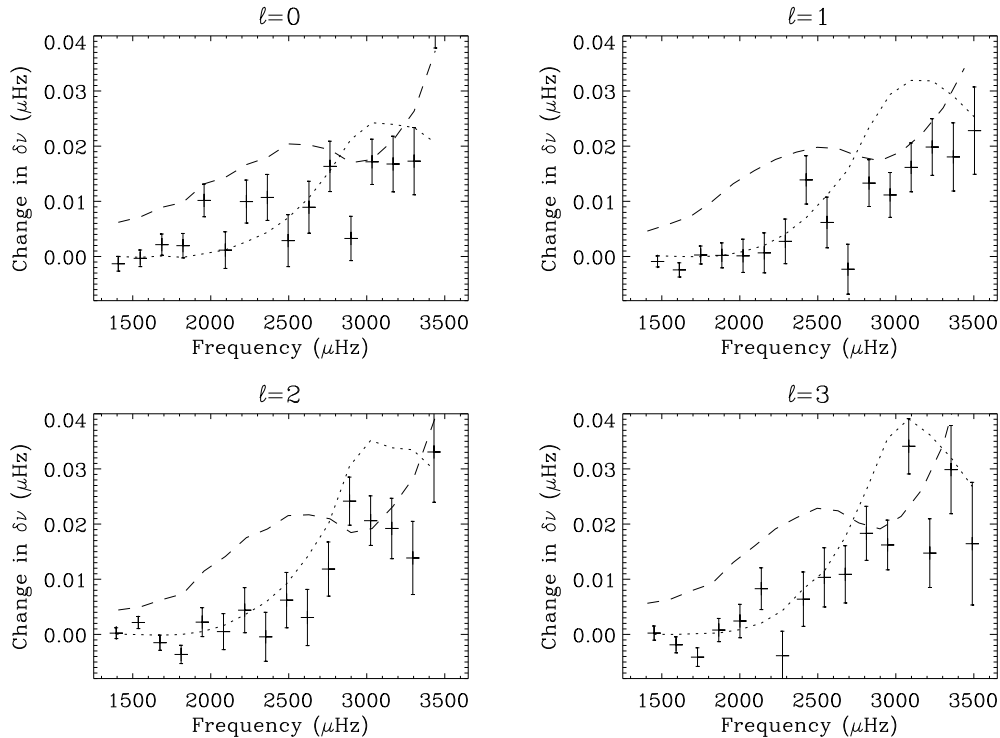


**Figure 4.** Dotted lines: sizes of the devil-in-the-detail effect, i.e., amounts by which the fitted frequencies are expected to be reduced compared to the unweighted average frequencies. Points with associated error bars: differences between the mean fitted FLAG#0 and FLAG#1 frequencies. Dashed lines: sizes of the typical frequency uncertainties expected from a single 9.5-yr dataset.

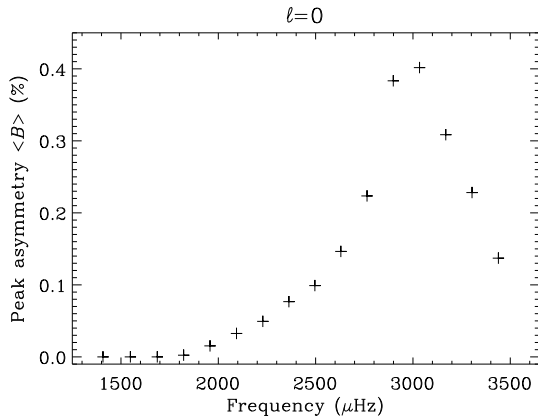


**Figure 5.** Peak asymmetry, from the devil-in-the-detail effect, that was given to artificial  $l = 0$  modes in the 9.5-yr FLAG#1 simulations.

## 5 CONCLUSIONS

Over the course of the solar cycle, variations are observed not only in the  $p$ -mode frequencies, but also in the  $p$ -mode powers. Variation of the powers over time gives rise to a cross-talk effect with the varying frequencies, which we call the devil-in-the-detail effect.

The effect, and its impact, may be summarized as follows. In the absence of any power variation, the location in the power frequency spectrum of the centroid of a mode peak would in principle give an accurate measure of the unweighted average mode frequency over the period of observation. However, when significant time variation of the power is present, data samples from times

when the mode is more prominent (i.e., at high power) will carry proportionately larger weights in determining the final peak profile than samples from times when the mode is less prominent (i.e., at low power). As the level of solar activity rises, the frequencies of the low- $l$   $p$  modes under study here increase, but corresponding mode powers decrease. This means that, for a long timeseries, the frequency of a mode peak will be biased so it is *lower* than the unweighted time-averaged frequency. This is our so-called devil in the detail.

### 5.1 Impact on Sun-as-a-star data

We have used extensive Monte Carlo simulations to estimate the magnitude of the resulting devil-in-the-detail bias, in BiSON- and GOLF-like Sun-as-a-star helioseismic data spanning almost one full activity cycle. Our simulations imply the bias should rise monotonically in frequency up to  $\approx 3000 \mu\text{Hz}$ , and then level off, or even decrease slightly in magnitude, at higher frequencies. It is at approximately the same frequency that the magnitude of the bias reaches a size that is comparable to the expected frequency uncertainties. Should we be worried by this devil-in-the-detail effect? Let us consider briefly, in this and the next section, two issues where the effect might be a potential cause for concern.

There is the impact of the effect on attempts to correct the frequencies for solar activity. Since our in-depth analysis has been made for Sun-as-a-star data on the low- $l$   $p$  modes, we are in a position to comment in detail on correction procedures for these data. Procedures which attempt to ‘remove’ the solar-cycle effects from the fitted frequencies (e.g., the BiSON correction procedure; see Basu et al. 2007) assume that the observed mode frequencies

correspond to unweighted time averages of the frequencies. The devil-in-the-detail effect therefore introduces a bias in the correction, which will be comparable in size to the frequency uncertainties for modes at frequencies above  $\approx 3000 \mu\text{Hz}$ . Will this also be true for analysis of resolved-Sun data on modes of higher  $l$ ?

## 5.2 Brief discussion on $l$ dependence of effect

The issue of the  $l$  dependence of the effect is of course important where inversions for the internal structure are concerned, since those inversions must make use of data on modes covering a wide range in  $l$ . It is a potential complication not just for analysis of non-contemporaneous data from two instruments (or more); but also for analysis of data from a single instrument, since significant variation of the bias with  $l$  could affect the accuracy of inversions. The impact of the bias on analysis of medium and high- $l$  data, from resolved-Sun observations, will be covered in detail in a future paper. Here, in order to get a feel for the likely size of the bias, its variation with  $l$ , and the possible impact on structure inversions, we conducted the following experiment.

First, we estimated the size of the devil-in-the-detail bias for different  $l$  in the range  $0 \leq l \leq 150$ , but only at fixed frequency (here, a notional mode frequency of  $3000 \mu\text{Hz}$ ). We assumed the frequency shifts should scale inversely with the mode inertias (and used the model ‘S’ inertias; see Christensen-Dalsgaard et al. 1996); and we estimated the  $l$ -dependent mode height and linewidth changes from GONG data analyzed in Komm, Howe & Hill (2000) [their Figs. 10 and 11]. With estimates of the solar-cycle frequency, height and linewidth changes to hand for each  $l$ , we were in a position to use Equation 3 to construct the expected final peak profiles – assuming a timeseries of length 9.5 yr (as in Sections 3.2 and 4) – and to thereby estimate the devil-in-the-detail bias as a function of  $l$ . Our results showed little variation of the estimated bias with  $l$  below  $l \lesssim 60$  (it being  $\approx 0.02 \mu\text{Hz}$  in size). However, at higher degrees the bias increased in a linear manner with increasing  $l$ , reaching a size of  $\approx 0.05 \mu\text{Hz}$  at  $l \sim 150$ .

Next, we scaled the estimated bias for each  $l$  by the inertia ratio of Christensen-Dalsgaard & Berthomieu (1991), and compared these scaled differences with sizes of scaled frequency differences that are typically large enough to affect inversion results for the internal structure at the  $1\sigma$  level (see also Eff Darwich et al. 2002). This assumed that the observed p-mode frequencies came from the MDI frequency set of Korzennik (2005), which includes frequencies on modes from  $0 \leq l \leq 125$ . The results of this comparison suggest that the devil-in-the-detail bias is not quite large enough to affect the inversions at the  $1\sigma$  level, although the amounts by which it fell short were marginal.

So, our preliminary conclusion, regarding the impact of the  $l$  dependence, is that the devil in the detail may not be a cause for concern where inversions for structure using data from a single instrument are concerned. That said, we should stress that this comparative analysis was an approximate one. At no point did we account for any possible  $m$  dependence, which might have a significant influence on the results. Without having done a full Monte Carlo simulation of the data, we were not in a position to provide an accurate estimate of the frequency dependence for different  $l$ . These factors will be tested in upcoming work.

## ACKNOWLEDGMENTS

SJJ-R, WJC, YE and RN acknowledge the support of the UK Science and Technology Facilities Council (STFC). SJJ-R also thanks

the European Helio- and Asteroseismology (HELAS) Network for support. HELAS is a major international collaboration funded by the European Commission’s Sixth Framework Program. The NSO/Kitt Peak data, used as part of the artificial (solarFLAG) time-series construction, were produced cooperatively by NSF/NOAO, NASA/GSFC and NOAA/SEL. We thank the solarFLAG collaboration for use of its artificial data.

## REFERENCES

- Appourchaux T., Chaplin W. J., 2007, *A&A*, 374, 1264  
 Basu, S., Chaplin, W. J., Elsworth, Y., New, R., Serenelli, A. M., Verner, G. A. 2007, *ApJ*, 655, 660  
 Chaplin, W. J., Elsworth, Y., Isaak, G. R., McLeod, C. P., Miller, B. A., New, R., 1997, *MNRAS*, 287, 51  
 Chaplin, W. J., Elsworth, Y., Isaak, G. R., Miller, B. A., New, R., 2000, *MNRAS*, 313, 32  
 Chaplin W. J., Appourchaux T., Elsworth Y., Isaak G. R., Miller B. A., New R., 2004, *A&A*, 424, 713  
 Chaplin W. J., 2006, *MNRAS*, 369, 985  
 Chaplin, W. J., Elsworth, Y., Miller, B. A., New, R., Verner, G. A., 2007, *ApJ*, 659, 1749  
 Chaplin W. J., Basu S., 2008, *Sol Phys*, in press  
 Chaplin W. J., Elsworth Y., New R., Toutain T., 2008, *MNRAS*, in press  
 Christensen-Dalsgaard, J., Berthomieu, G. 1991, in *Solar Interior and Atmosphere*, eds. A.N. Cox, W.C. Livingston, M.S. Matthews, University of Arizona Press, Tuscon, p401  
 Christensen-Dalsgaard, J., et al. 1996, *Science*, 272, 1286  
 Eff-Darwich A., Korzennik S. G., Jiménez-Reyes S. J., Pérez-Hernandez F., 2002, *ApJ*, 580, 574  
 Fröhlich, C., Andersen, B.N., Appourchaux, T., et al. 1997, *Sol Phys*, 170, 1  
 Gabriel, A.H., Grec, G., Charra, J., et al. 1995, *Sol Phys*, 162, 61  
 Jiménez-Reyes, S. J., García, R. A., Chaplin, W. J., Korzennik S., 2004, *ApJ*, 610, L65  
 Jiménez-Reyes, S. J., Chaplin, W. J., Elsworth, Y., García, R. A., Howe, R., Socas-Navarro, H. Toutain, T., 2007, *ApJ* 654, 1135  
 Komm R., Howe R., Hill F., 2000, *ApJ*, 531, 1094  
 Korzennik S. G., 2005, *ApJ*, 626, 585  
 Nigam, R. & Kosovichev, A. G., 1998, *ApJ*, 505, L51  
 Salabert D., Chaplin W. J., Elsworth Y., New R., Verner G. A., 2007, *A&A*, 463, 1181  
 Simoniello R., Chaplin W. J., Elsworth Y., Isaak G. R., New R., 2004, *ApJ*, 616, 594

## APPENDIX A: VARIATION OF ARTIFICIAL MODE PARAMETERS

A useful model for the solar p modes is a forced, damped harmonic oscillator. The artificial data described in the paper are based on oscillators described by the equation:

$$\ddot{x}(t) + 2\eta(t)\dot{x}(t) + [2\pi\nu(t)]^2 x(t) = K(t)\delta(t - t_0). \quad (\text{A1})$$

Here:  $x(t)$  is the displacement of the oscillator;  $\nu(t)$  is its cyclic frequency;  $\eta(t)$  is the linear damping rate; and  $K(t)$  is the amplitude of the forcing function (the ‘kick’), which is drawn from a Gaussian distribution with zero mean and variance  $\sigma_K(t)$ , i.e.  $K(t) \sim N[0, \sigma_K(t)]$ .



Here, we have given the basic oscillator parameters an explicit dependence on  $t$  to indicate the parameters are varied in simulated time. It can be shown (e.g., Chaplin et al. 2000; see also Simoniello et al. 2004) that the implied instantaneous maximum power spectral density at time  $t$ , of a timeseries of the oscillator velocity  $\dot{x}(t)$ , is described by:

$$H(t) \propto \frac{\sigma_K^2(t)}{\eta^2(t)}. \quad (\text{A2})$$

In the first simulation scenario in Section 2, where  $\sigma_K(t)$  was varied in time but  $\eta(t)$  remained fixed, we therefore have:

$$H(t) \propto \sigma_K^2(t), \quad (\text{A3})$$

so that

$$\Delta H/H(0) = 2\Delta\sigma_K/\sigma_K(0). \quad (\text{A4})$$

In the second simulation scenario in Section 2, where  $\eta(t)$  was varied in time but  $\sigma_K(t)$  remained fixed, we have:

$$H(t) \propto 1/\eta^2(t),$$

$$\Gamma(t) \propto \eta(t). \quad (\text{A5})$$

Therefore:

$$\Delta H/H(0) = -2\Delta\eta/\eta(0),$$

$$\Delta\Gamma/\Gamma(0) = \Delta\eta/\eta(0). \quad (\text{A6})$$

So, in the second scenario both the height *and* linewidth change in time. The fractional variation in the height is twice that in the width, and the fractional changes have opposite sign.